Combining surface drifters and high resolution global simulations enables the mapping of internal tide surface energy

Zoé Caspar-Cohen

zcasparcohen@ucsd.edu

Scripps Institution of Oceanography

Aurélien Ponte

Laboratory for Ocean Physics and Satellite Remote Sensing

Noé Lahaye

Inria Rennes - Bretagne Atlantique Research Centre

Edward D. Zaron

College of Earth, Ocean and Atmospheric Sciences

Brian K. Arbic

Department of Earth and Environmental Science

Xiaolong Yu

School of Marine Science

Sylvie LeGentil

Laboratory for Ocean Physics and Satellite Remote Sensing

Dimitris Menemenlis

Jet Propulsion Laboratory

Article

Keywords:

Posted Date: July 2nd, 2024

DOI: https://doi.org/10.21203/rs.3.rs-4583670/v1

Additional Declarations: No competing interests reported.

Combining surface drifters and high resolution global simulations enables the mapping of internal tide surface energy

Zoé Caspar-Cohen *[1,2,3], Aurélien Ponte[2], Noé Lahaye[3], Edward D. Zaron[4], Brian K. Arbic[5], Xiaolong Yu[6], Sylvie LeGentil[2], and Dimitris Menemenlis[7]

[1]Scripps Institution of Oceanography, University of California San Diego

[2]Univ Brest, CNRS, Ifremer, IRD, Laboratoire d'Océanographie Physique et Spatiale (LOPS), IUEM, F29280, Plouzané, France.

[3]Odyssey team, Inria & IRMAR, Campus Universitaire de Beaulieu, Rennes, France

[4]College of Earth, Ocean, and Atmospheric Sciences, Oregon State University, Corvallis, OR, USA

[5]Department of Earth and Environmental Sciences, University of Michigan, Ann Arbor, MI, 48109

[6]School of Marine Sciences, Sun Yat-sen University, Zhuhai, China

[7]Jet Propulsion Laboratory, California Institute of Technology, Pasadena, CA, USA

June 2024

Abstract

By dissipating energy and generating mixing, internal tides (ITs) play a major role in the climatological evolution of the ocean. Our understanding of this class of ocean variability is however hindered by the rarity of observations capable of capturing ITs with global coverage. The data provided by the Global Drifter Program (GDP) offer high temporal resolution and quasi-global coverage, thus bringing promising perspectives. However, due to their inherent drifting nature, these instruments provide a distorted view of the IT signal. By theoretically rationalizing this distortion and leveraging a massive synthetic drifter numerical simulation, we are able to map semi-diurnal IT energy levels from GDP data and compare it to three datasets (two numerical simulations, and a satellite altimetry IT atlas). We find that all numerical simulations exhibit biases. Nonetheless, the simulation that benefited from dedicated attention towards ITs representation performs best. This supports renewed efforts in the concurrent numerical modeling of ITs / ocean circulation. The substantial deficit of energy in the IT atlas highlights the inability for altimetric

estimates to measure incoherent and finer scale ITs and strongly supports the need to isolate ITs signature in the data collected by the new wide-swath altimetry mission SWOT.

1 Introduction

Internal tides (ITs) are a key component of the ocean circulation, as they cause dissipation and mixing, thereby impacting the large scale ocean circulation (Munk and Wunsch, 1998; Ferrari and Wunsch, 2009; Melet et al., 2013; Whalen et al., 2020). Their importance has been recognized for decades and their explicit representation in ocean general circulation models is possible and has been improving for the last decade (Arbic et al., 2010, 2018). Moreover, the surface signature of ITs has been flagged as a major issue for the exploitation of emerging satellite sensing – in particular for the Surface Water Ocean Topography (SWOT) mission (Arbic et al., 2015) – as they overlap with the signature of non-wave motions at the submesoscale, while temporal filtering is prevented by the coarse temporal sampling. Understanding internal tide dynamics and quantifying its energetics are therefore of crucial importance and remain insufficient to date.

ITs can propagate over long distances and, in doing so, interact with the turbulent background ocean populated with unsteady jets and eddies. These interactions alter IT propagation and result in a loss of coherence (reduction of phase-locking with the generating source – the barotropic tide). Part of the IT signal will then be incoherent (non phase-locked), characterized by an incoherent IT variance and an incoherent time scale. As a consequence, the ITs estimates based on sea level measurements from satellite altimetry, which rely on multi-years long time series to dealias IT high-frequency signals, are limited to their coherent contribution and missing part of the IT signal (Zaron et al., 2022; Zhao et al., 2012). Estimates of total (coherent and incoherent) semi-diurnal tide variance have been obtained from along-track altimetry data (for mode-1 IT) (Zaron, 2017), and using Argo floats measurements (Geoffroy and Nycander, 2022), moorings (Luecke et al., 2020) and cruises (Rocha et al., 2016). Estimates of the incoherent tide variance, based on along-track altimetry data and Argo floats, were found to reach from 44% to 85% of the total energy (Zaron, 2017; Geoffroy and Nycander, 2022). These estimates are however limited to specific areas due to the restrained spatial coverage.

Numerical models have recently become able to explicitly represent internal tide fields in high resolution realistic simulations of order a year long and at basin or global scale (Arbic, 2022). The comparison of numerical simulations to other datasets, notably moorings (Luecke et al., 2020) or altimetry (Nelson et al., 2019), supports their potential to simulate both coherent and incoherent internal tides. While these simulations provide valuable insights on the IT dynamics, it has been shown that numerical aspects such as parameterized wave drag can have a strong impact on the simulated IT field (Buijsman et al., 2020). To validate these numerical models, and complement satellite altimetry, continuing effort to find appropriate data is called for in order to identify the total global IT kinetic energy, i.e., including both coherent and incoherent internal tides for all vertical modes.

In that regard, the quantification of the IT field through globally deployed surface drifters from the Global Drifter Program, GDP, (Elipot et al., 2016) is particularly relevant. Indeed, it provides hourly data of the drifter position, from which currents can be estimated across a wide range of time scales (including motions at the typical semi-diurnal tide period of $\sim$ 12 h) at global scale. Estimates of kinetic energy in the tidal frequency bands are thus possible from this dataset (Yu et al., 2019; Arbic et al., 2022). However it has been identified that the Lagrangian – i.e. along-flow – perspective can bring some distortion with respect to the Eulerian – i.e. fixed-point – one (Zaron and Elipot, 2021; Caspar-Cohen et al., 2022). This distortion, coined "apparent incoherence", must therefore be addressed if one seeks a reliable estimate of the internal tide energy to compare to Eulerian estimates.

We show here how drifter data may be used to estimate total semi-diurnal internal tides energy levels. We propose a method to compensate the Lagrangian bias in drifter diagnostics and map internal tide surface kinetic energy from the GDP hourly dataset. Using a state-of-the-art high-resolution numerical simulation of the world ocean, the Massachusetts Institute of Technology general circulation model (MITgcm) LLC4320, populated with surface Lagrangian particles, we first construct model-based maps of IT surface kinetic energy and identify the relationship between Lagrangian and Eulerian diagnostics. We then propose and validate a simple conversion accounting for the Lagrangian distortion, that allows us to "debias" Lagrangian-based kinetic energy estimates. These debiased estimates are then compared with estimates from numerical models (MITgcm and the Hybrid Coordinate Ocean Model – HYCOM) and from altimetry data (High Resolution Empirical Tide – HRET).

2 Results

Quantifying and explaining Lagrangian biases with high resolution simulation and theory

The state-of-the-art global tide resolving numerical simulation LLC4320 (based on the MITgcm model; NASA 2021) and a synthetic drifter release based on LLC4320 velocity outputs are leveraged to produce a unique comparison between Eulerian (fixed-point) and Lagrangian (drifter/along-flow) semi-diurnal internal tide kinetic energy (Figure 1, section 4). As, expected, both Lagrangian (Fig. 1a) and Eulerian (Fig. 1b) energy levels exhibit maxima at internal tide generation hotspots, near oceanic ridges and islands (e.g., mid-ocean ridges, South China Sea, etc.) with values up to $\sim$0.015 m^2 s^{-2}. A global reduction of drifter energy levels is observed compared to Eulerian ones, with an average of approximately 75% of the Eulerian energy recovered in the Lagrangian framework (Fig 1 and Fig 2 a and b). This could impact our ability to compare drifters observation and Eulerian-based estimates and needs to be explained and accounted for.

The Lagrangian to Eulerian energy ratio is referred to as "estimated energy ratio" in the rest of the study. This ratio varies geographically, ranging from about 0.5 to unity. It is clearly modulated by the intensity of low frequency motions with lowest energy ratio observed in low frequency energetic areas, e.g. Equatorial currents, Gulf Stream, Kuroshio (Figure 2 a). Caspar-Cohen et al. (2022) provides an explanation for this sensitivity of the bias between Lagrangian and Eulerian energy levels to the low-frequency flow magnitude, which relies on the combination between the distortion of ITs temporal signature induced by drifters' motions relative to ITs horizontal structure, on the one hand, and, the filtering of the velocity signal in a fixed frequency band on the other hand. The former effect is related to the displacement-induced projection of spatial variability into the temporal one, which is a well-known and more general feature associated with Lagrangian observations (LaCasce, 2008). The magnitude of this distortion thus depends on the distance traveled by a drifter over an IT time period relative to the IT horizontal wavelength, and this distance directly depends on the mean flow strength (Figure 3 left panels). Caspar-Cohen et al. (2022) showed that the distortion leads to more rapid modulations of ITs which, in the frequency domain, translates into wider peaks in the Lagrangian spectra (Fig. 3, right panels and Fig. S2 in Supplementary information). Once integrated across the IT frequency band, Lagrangian kinetic energy estimates will thus tend to be weaker than Eulerian estimates. In the case of small drifter displacements (labeled (A) in Figure 3), the drifter behaves as an Eulerian observer (e.g. a mooring) and measures purely temporal fluctuations. Lagrangian and Eulerian spectra match (Fig. 3, label A, right panel), resulting in similar band-integrated energy levels. Conversely, in the case of large drifter displacements (labeled (B) in Figure 3), the wave spatial variability is projected into the temporal one, resulting in apparent incoherence with wider Lagrangian spectral peaks compared to Eulerian ones (Fig. 3, label B, right panel), and ultimately lower Lagrangian energy estimates. This effect is mainly limited to 75% of the Eulerian energy, but can be stronger in regions of strong currents (such as some of the ones previously listed).

The apparent incoherence theoretical model of Caspar-Cohen et al. (2022) is further exploited to predict the Lagrangian to Eulerian kinetic energy ratio – referred to as "predicted energy ratio" (Fig. 2c and d). Its prediction is further described in section 4. Estimated and predicted energy ratios compare well visually with predictions of energy ratio minima in terms of their values (~ 0.5) and locations. This strongly supports the fact that the smaller Lagrangian-based estimates are indeed linked to apparent incoherence and purely caused by the entanglement of spatial and temporal variability in Lagrangian-based estimates and the associated widening of Lagrangian spectra. A conversion from Lagrangian to Eulerian framework is thus necessary in order to compare them to Eulerian-based estimates.

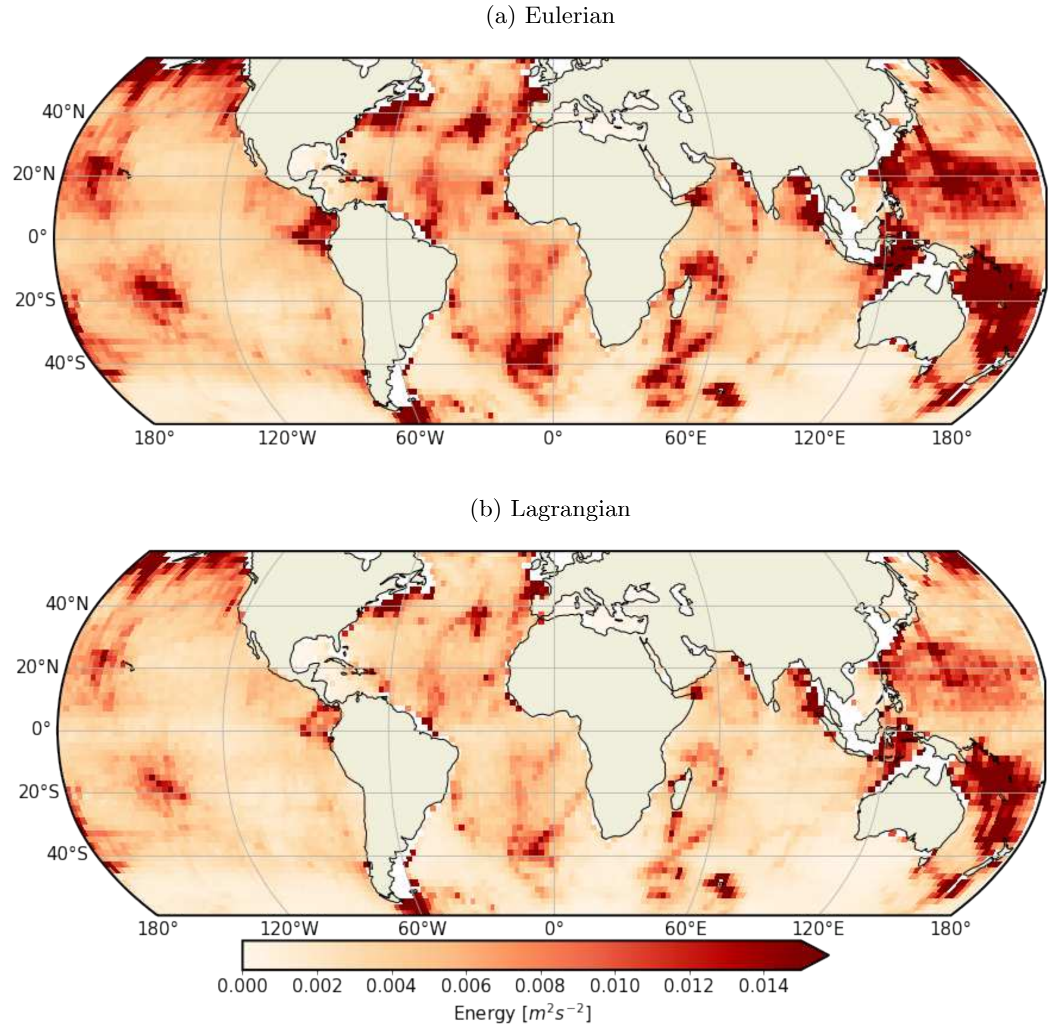

Figure 1: Maps of (a) Eulerian and (b) Lagrangian kinetic energy levels in the semi-diurnal band computed from LLC4320 surface outputs and simulated drifter trajectories. The energy levels are averaged over time and over 2°x2° spatial bins.

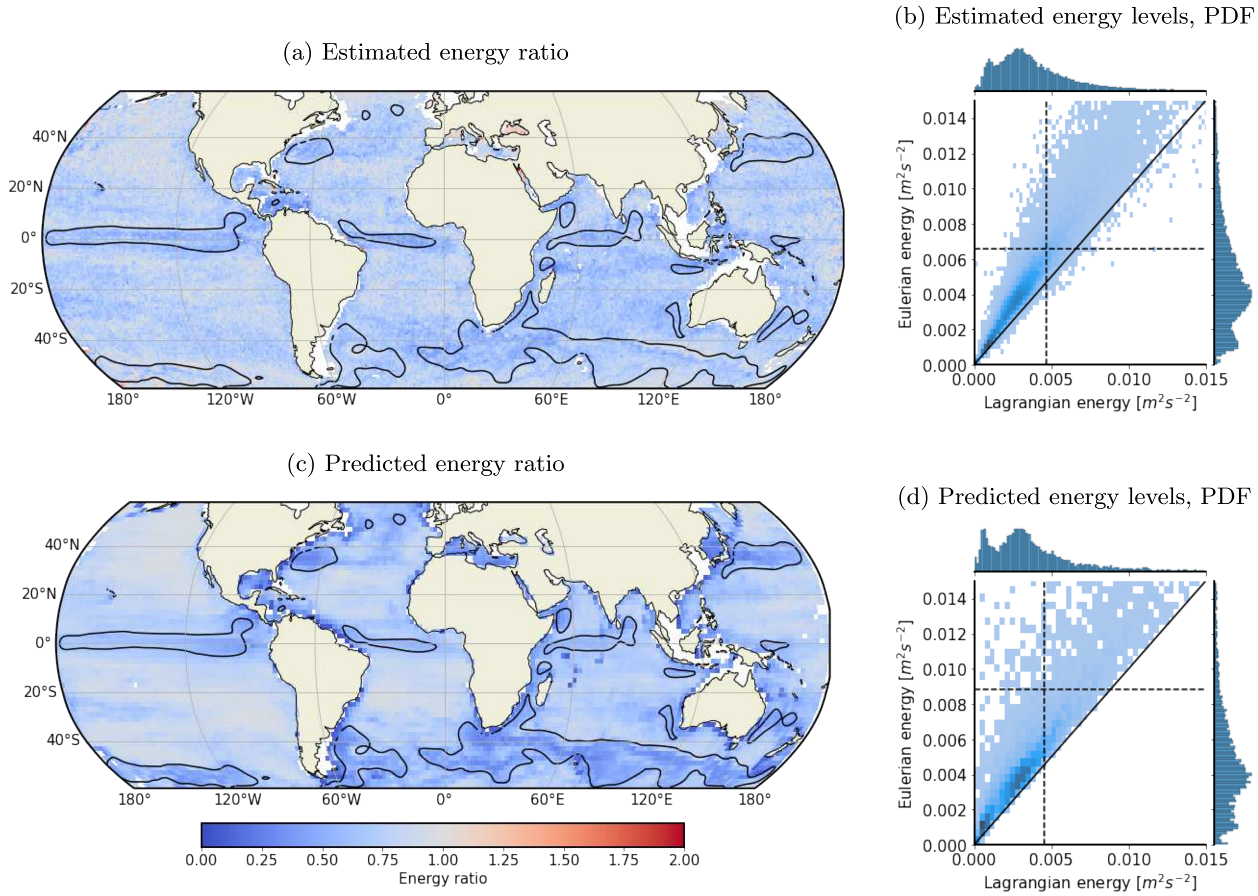

Figure 2: Comparison between estimated Eulerian kinetic energy (from LLC4320) and estimated / predicted Lagrangian kinetic energy. Maps of (a) estimated and (c) predicted Lagrangian to Eulerian energy ratio in the semi-diurnal band computed from LLC4320 surface outputs and simulated drifter trajectories. Black contours define regions in which the low frequency kinetic energy is larger than 0.1 m^2 s^{-2}. Joint plots of the distribution of (b) estimated and (d) predicted (x-axis) Lagrangian and (y-axis) Eulerian energy levels are also plotted in the right panels. Dashed black lines represent mean Eulerian and Lagrangian energy values.

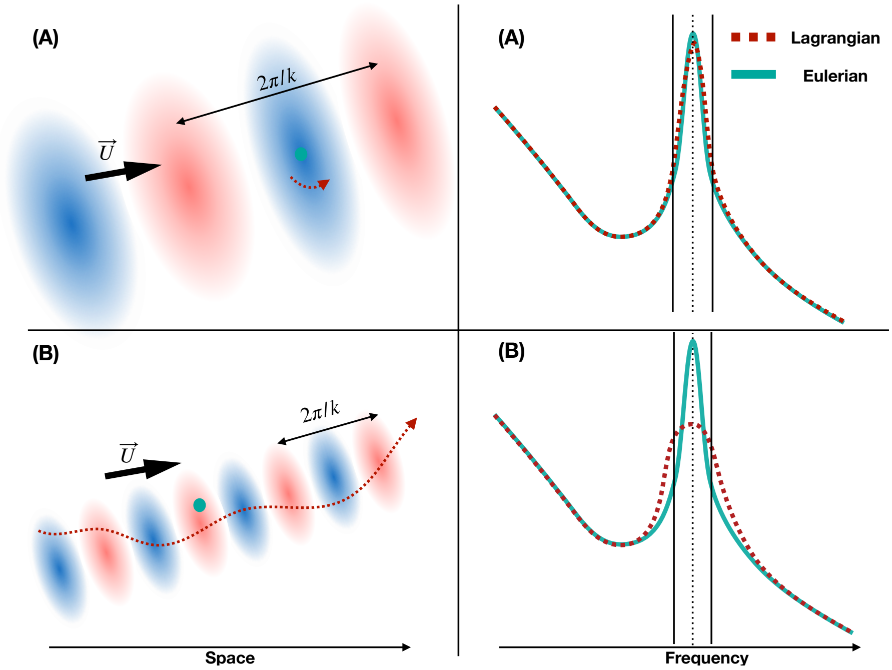

Figure 3: Schematic description of the bias introduced by drifter displacements and how this bias impacts the energy levels found in a fixed frequency band. Two examples are shown, labeled (A) and (B). (A) corresponds to weak and (B) to strong drifter advection by the low-frequency background flow. Left panels represent the waves signature and the drifter displacement, represented by the dashed red curve, compared to the wavelength $2\pi/k$. $\vec{U}$ represents the background low-frequency flow. Right panels represent the same case scenario in the frequency domain with schematic power spectra around a central frequency (represented by the dotted line). Solid vertical black lines correspond to the limits of a fixed frequency band.

Applications: comparing Eulerian datasets to ground truth energy levels

Now that the differences between Eulerian and Lagrangian-based energy estimates have been rationalized and predicted, we introduce a conversion factor to obtain reference energy levels from global, high temporal resolution in situ drifter dataset. In accordance with theory, we assume that the Lagrangian to Eulerian energy ratio depends on the strength of the low-frequency flow (defined as motion with timescales larger than 2 days) and internal tide spatial scales, both of which we assume are correctly predicted in the LLC4320 simulation (see Yu et al. (2019) for a quantitative description). This ratio can then be used as a conversion factor for Lagrangian observations. From there, converted Eulerian-like energy estimates (Figure S1a in Supplementary information) are obtained by multiplying Lagrangian-based energy levels with the conversion factor (Figure 2a).

This conversion is thus applied to the energy estimate from the in situ Lagrangian observations of hourly surface velocity provided by the GDP (Elipot et al. (2016, 2022), section 4). The converted energy levels (GDPC) may be used as reference energy levels and compared to Eulerian-based estimates giving us a unique tool to directly validate and complement estimates from numerical models and along-track altimetry. We next use energy levels estimated in the same frequency band in two high resolution global numerical simulations, LLC4320 (Figure 4 a) and HYCOM (Arbic 2022; Arbic et al. 2022; Figures 4b and S1b in Supplementary information, and section 4). In addition, we compare our dataset to estimates from altimetry (Zaron et al. 2022; Figure 4c).

Despite similar input data types and processing, both numerical simulations exhibit significant differences when compared to semi-diurnal converted energies. LLC4320 energy levels overall overestimate GDP converted energy levels by a factor 2 on average (Figure 4a). Both LLC4320 and converted GDP energy levels follow a similar dependence on latitude (Figure 5 yellow and red curves), supporting the hypothesis of general phenomena causing this overestimation. Arbic et al. (2022) attributed this issue to the lack of a parameterized topographic internal wave drag in LLC4320 which has been shown to be necessary for accurate tides in HYCOM (Arbic et al., 2010; Ansong et al., 2015; Buijsman et al., 2020; Arbic, 2022). Comparing simulation outputs to converted energy levels instead of the biased (e.g., Lagrangian) ones attenuates this overestimation, decreasing from a factor 3 of the original dataset to a factor 2 of the converted one (Figure 4a, right panel). In comparison, the HYCOM simulation shows a better match with converted energy levels, representing 87% of converted levels. Differences between HYCOM and converted GDP energies highlight regional differences with, for instance, an underestimation below 40°S where HYCOM energy levels represents 37% of the GDP energy, and an overestimation in the North eastern Pacific area (energy levels five times higher than the converted GDP energy). Arbic et al. (2022) attributed the latter anomaly to numerical instabilities. The area between -30° and 30°N shows a particularly good concordance with converted levels, visible especially in the zonal average (Figure 5 green and red curves), with an average overestimation of the converted GDP energy by a factor 1.03, i.e., only 3% difference compared to GDPC energies. The comparison of our converted dataset to this simulation highlights again the importance of the conversion process as energy levels would have been overall overestimated in HYCOM if compared directly to GDP energy levels, 87% of converted levels vs. 117% of the original GDP dataset.

Reference energy levels also open the door to the quantification of IT incoherent energy fractions. Due to their low temporal resolution, IT atlas derived from satellite altimetry are indeed limited to coherent IT and few vertical modes. The incoherent energy has been estimated previously to account for a significant fraction of the total tidal energy 44% (Zaron, 2017) to 68% (Nelson et al., 2019). This remains true even in the case of advanced products such as High Resolution Empirical Tide (HRET) (Zaron et al., 2022). Indeed, while HRET successfully represents IT generation hotspots and main area of interest (Figure 1c in Supplementary information), its energy levels strongly depend on its ability to include incoherent and high modes tides in this representation. In the case of mode-1 internal tides and considering only the two main components, M_2 and S_2, kinetic energy from HRET represents only 11% of the reference energy levels (Figures 4c and 5 blue curve). As further discussed in sections 3 and 4, the fundamental difference of data processing between HRET and GDP dataset explains this large difference. This result highlights the significance of including incoherent and/or contributions of higher modes as well as the necessity to use in situ observations to complement satellite altimetry.

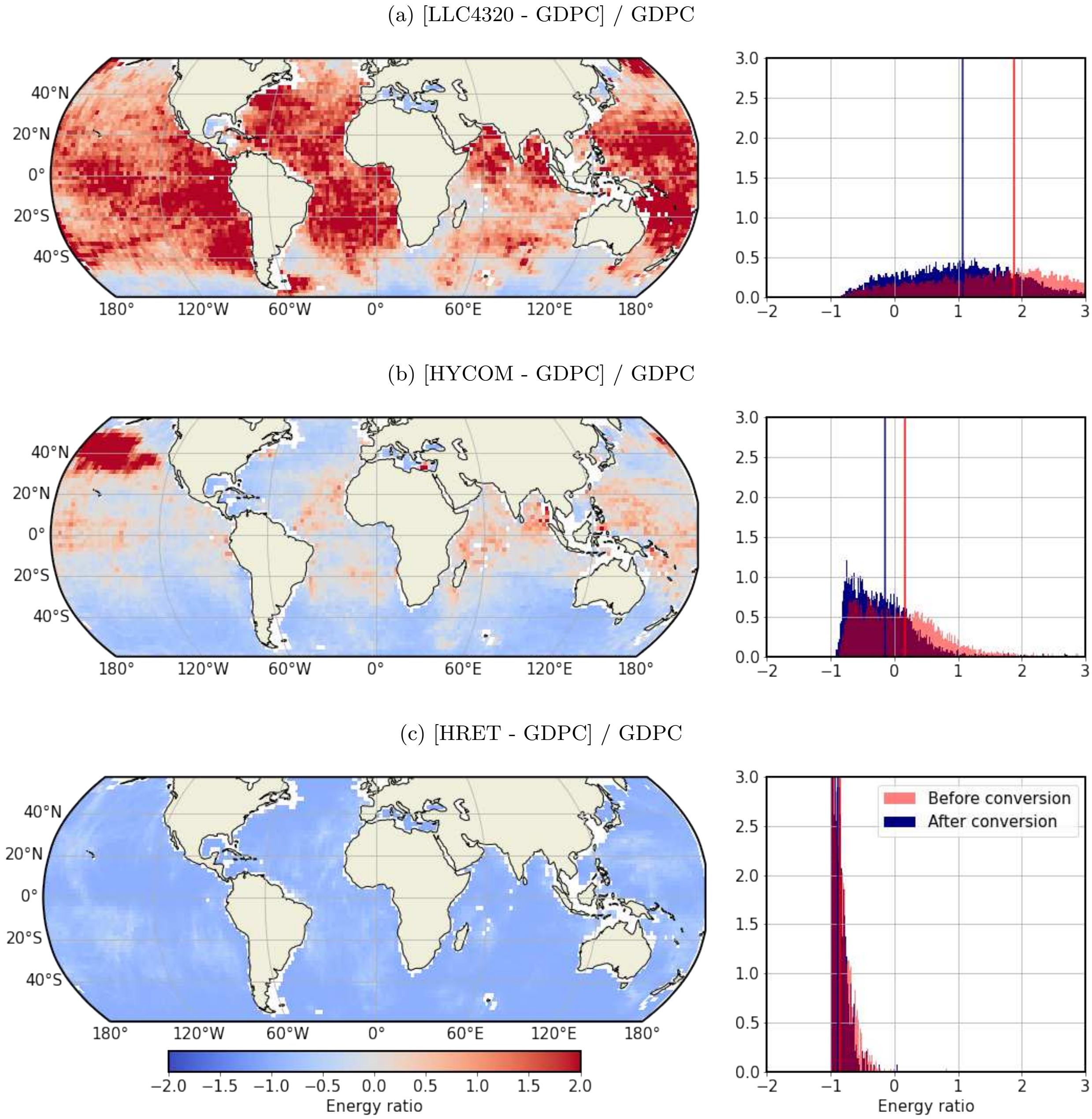

Figure 4: Comparison of semi-diurnal kinetic energy estimated from GDP dataset to the ones from LLC4320, HYCOM and HRET. (Left panels) Maps of the surface semi-diurnal kinetic energy differences between (a) LLC4320, (b) HYCOM and (c) HRET and the converted energy levels from GDP surface drifters normalized by converted GDP energy levels. (right panels) The distributions of the difference between each dataset and (blue) converted and (red) biased energy levels from GDP data are shown. Mean energy differences are represented by the colored vertical lines.

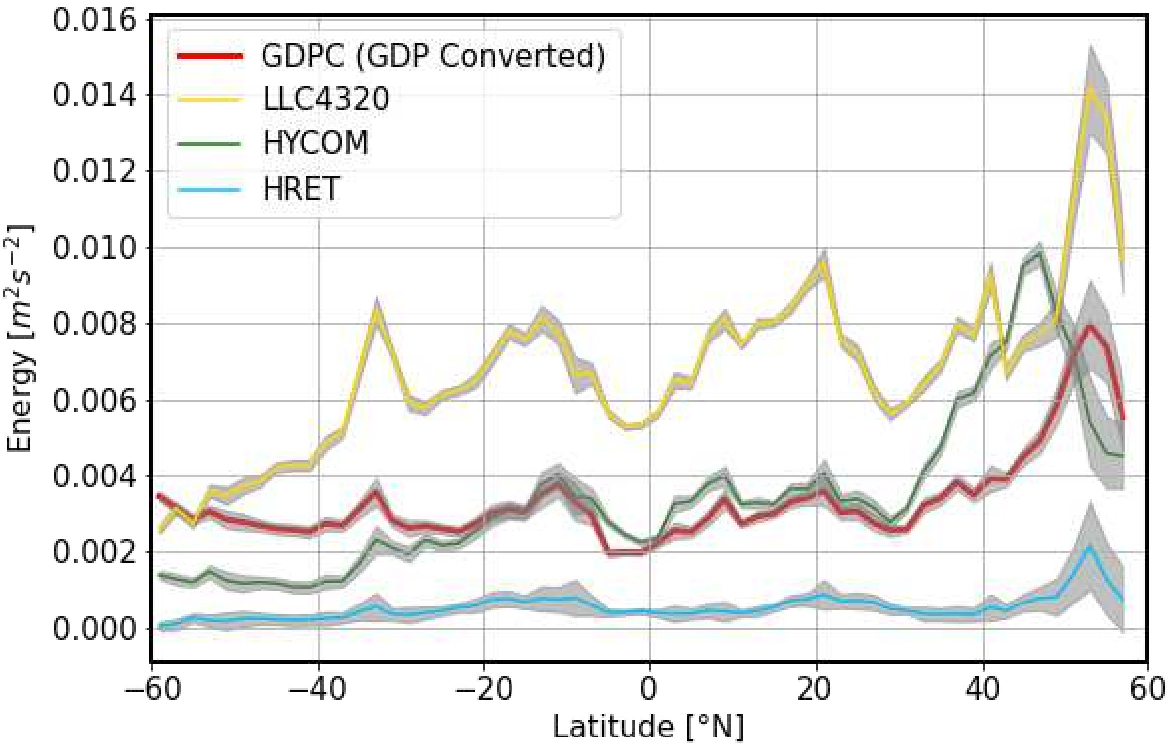

Figure 5: Zonal average of the surface semi-diurnal kinetic energy estimated from LLC4320, HYCOM, converted GDP and HRET. Grey shading correspond to error due to spatial sampling (i.e. standard deviation)

3 Discussion

Our study confirms the relevance of apparent incoherence for Lagrangian based mapping of the semi-diurnal internal tide. Its existence was speculated by Zaron and Elipot (2021) and Arbic et al. (2022) and verified in idealized simulations and modeled theoretically by Caspar-Cohen et al. (2022). Apparent incoherence and the associated spectral widening of the semi-diurnal peak resulting from drifter displacements is found to lead, without adequate treatment, to an average low bias of 25% of semi-diurnal Lagrangian-based estimated when compared to Eulerian-based ones. This difference is the largest in areas of energetic low frequency variability, where Lagrangian energy levels represents only 60% of the Eulerian energy levels, in accordance with theoretical predictions.

Motivated by this successful theoretical description, we proposed a conversion of the GDP based estimates of semi-diurnal energy distribution to an Eulerian-like distribution. This method relies on the comparison between Lagrangian and Eulerian semi-diurnal energy levels in a state of the art numerical simulation of the ocean circulation. Our approach essentially remains robust to an overall bias in semi-diurnal variability energy, but critically assumes that the numerical simulation is able to reproduce the internal distribution across spatial scales. The latter assumption could be partly tested in latter studies at isolated spots with mooring data (Timko et al., 2012, 2013; Wang et al., 2018; Luecke et al., 2020), or altimetric observations via coherent internal tides (Ray and Mitchum, 1996, 1997; Zhao, 2014; Pan et al., 2022).

This original approach enabled us to reassess the accuracy of the semi-diurnal internal tide variability predicted by two global tide-resolving numerical predictions (MITgcm LLC4320 and HYCOM). Previous results are confirmed: MITgcm LLC4320 semi-diurnal energy is higher than in situ observations by a factor of about two on average (equivalent to 8×10^{-3} m^2 s^{-2}). HYCOM exhibits relatively little bias on average but regional modulations emerge: underestimated energy outside the tropics, overestimation in the tropics, and anomalous energy excess in the North Pacific caused by numerical instability. Reference energy levels Eulerian-like estimates using a conversion of Lagrangian observations highlight models and areas for which configurations are seemingly best suited to successfully describe IT dynamics. In addition, our study emphasizes the need to carefully factor potential biases when using in situ observations to validate these simulations. This assessment of the accuracy of numerical simulations, in regard to IT kinetic energy, is potentially limited by the different temporal coverage between numerical simulations and GDP ($\sim$ one year against several decades). We argue that at least a year is covered by numerical simulations which mitigates seasonal fluctuations of the semi-diurnal IT energy (Lahaye et al., 2019). Inter-annual fluctuations however may remain and should be investigated in the future.

A second direct application of our estimate of semi-diurnal internal tide energy is to provide new estimates of the IT *incoherent* kinetic energy via comparisons with altimetry-based estimates of the coherent energy (HRET). The averaged incoherent, and modes higher than 1, energy is about 5×10^{-4} m^2 s^{-2}, which is 89% of the total energy on average. This metric may be leveraged to assess the ability of tidal models to reproduce coherent and incoherent internal tides independently, and constitute a useful background value for internal tide data assimilation efforts (Le Guillou et al., 2021b,a; Wang et al., 2022).

Two points that may be investigated in the future are the presence of non-tidal motions in the semi-diurnal frequency band, e.g., submesoscale low-frequency motions, and, on the contrary, the risk to exclude some of the tidal energy. Two parameters control this: the form of the spectra of low-frequency motions, mostly determined by the decorrelation timescale, and the width of the frequency band chosen for the data processing. An investigation showed that a theoretical spectral form for low-frequency motions and tests of different frequency bands could provide a satisfying frequency bandwidth (Fig. S3). This results in a generic choice that successfully reduced the fraction of low-frequency energy present in the semi-diurnal band and its impact on the comparison of Lagrangian datasets with Eulerian-based estimates. This choice could be more finely defined in local studies, where a more precise optimal bandwidth could be necessary. However, this fraction of energy and/or other source of contamination will change depending on the frequency of interest of a study and optimum bandwidth should be carefully defined for each study case.

Overall, this study highlights a recent surge of efforts and substantial results around the mapping of internal tides in the ocean in general and from drifter data in particular. Leads for future studies are numerous ranging from the application of present methods to diurnal tides (although apparent incoherence is expected to be weaker, as associated length scales are larger, and part of the signal may be non-tidal; Arbic et al. 2022), to per-vertical mode description of the effect of apparent incoherence. SWOT, its fast sampling phase in particular, may provide unprecedented details of internal tide dynamics which combined with drifter data could lead to unprecedented descriptions of the ocean internal tide variability. This could have a long-standing impact on our ability to represent internal tides explicitly in high resolution numerical simulations or implicitly via the parametrization of their effects in climate numerical simulations (Simmons et al., 2004; Melet et al., 2016; Olbers et al., 2019; de Lavergne et al., 2019).

4 Methods

LLC4320 and GDP data processing

LLC4320 is a global-ocean configuration based on the MIT general circulation model (MITgcm) (NASA, 2021). Its grid resolution is 1/48° horizontally, i.e., around 2 km (1 km in the Arctic, 2.4 km at the Equator) with 90 vertical levels. Outputs have been produced with hourly resolution. Atmospheric forcing is based on ECMWF 6 hourly product, and tides are forced with 16 major constituents. An erroneous 10% overestimation of the tidal forcing has been reported in Arbic et al. (2022). LLC4320 dataset is approximately one year long, beginning on the 15th of November 2011 and ending on the 9th of November 2012. Drifter trajectories are computed offline from the hourly surface velocity fields using Ocean Parcels (Van Sebille et al., 2018). Interpolation schemes are a 4th order Runge-Kutta in time and TRACMASS in space (Delandmeter and Van Sebille, 2019). Drifters are initially deployed every 50 grid points ($\sim$1°) in latitude and longitude. Every 10 days, drifters are released at initial drifter locations if the closest drifter exceeds the initial closest neighbor separation. The number of drifters in the simulation hence increases from about 60 000 to 100 000 at the end of year-long simulation. This reseeding strategy enables to obtain above 8000 drifter positions per 1°x1° spatial bin over the time series length outside of Equatorial area and above 5000 drifters at the Equator.

The in situ drifter dataset used in section 2 are the surface velocity fields provided by the GDP with a 1 hour time resolution. In our study data from both Argos and GPS-tracked drifters were used (Elipot et al., 2016).

The same data processing is applied to both simulated and in situ datasets in order to extract semi-diurnal variability from velocity time series. The first step is to bandpass filter the raw signal in the semi-diurnal frequency band defined by its central frequency $\omega_c = (\omega_{M_2} + \omega_{S_2})/2 \simeq 1.97$ cpd and bandwidth $\Delta\omega = 0.4$ cpd. The Hilbert transform is then applied to filtered time series. The resulting analytical signal is multiplied by $\exp(-i\omega_c t)$ leading to the demodulated tidal signal $\tilde{u}(t)$. As illustrated in Arbic et al. (2022), energy estimates may be sensitive to the choice of bandwidth. The present choice is motivated by synthetic experiments and results from a trade-off aiming at reducing the imprint of background energy while including the majority of the semi-diurnal tidal signal.

Averaged kinetic energy are then obtained from the demodulated horizontal velocity time series, $\tilde{u}$ and $\tilde{v}$ for the zonal and meridional velocity respectively. For Eulerian time series, this averaged energy is given by:

$$KE_{E,high} = \frac{1}{2} < \overline{\tilde{u}_E^2 + \tilde{v}_E^2} >_b \tag{1}$$

where $< . >_b$ is the horizontal bin average and $\bar{\cdot}$ is the time average. For Lagrangian model and in situ time series, the energy is computed according to:

$$KE_{L,high} = \frac{1}{2} < \tilde{u}_L^2 + \tilde{v}_L^2 >_{b,t} \tag{2}$$

where $< . >_{b,t}$ is the time and horizontal bin average.

HYCOM data processing

The dataset from the HYCOM simulation was processed outside of the scope of this study by Arbic et al. (2022) who give a complete description of both data and method. The HYCOM simulation has a 1/25° horizontal resolution with 41 vertical levels. The tidal forcing accounts for the 5 largest tidal components, including the three main semi-diurnal components, M2, S2, and N2. Outputs are provided with hourly time resolution for about one year starting on 1 January 2014.

Kinetic energy is estimated from frequency rotary spectra which are computed by splitting the complex velocity time series $u+iv$, where u and v denote zonal and meridional velocities respectively, into 60-day windows overlapping by 50% (Arbic et al., 2022). For each temporal window, time series are detrended and multiplied by a normalized Hann window. Individual discrete Fourier transform are then computed and multiplied by their complex conjugates. Averages over all windows and within 1°x1° bins lead to time-averaged kinetic energy spectra. These spectra are then integrated in the 1.8 to 2.2 frequency band, thereby providing the maps of kinetic energy presented in section 2.

The data processing differs from the one applied to LLC4320 and GDP datasets. In order to investigate the potential impact of this difference on the comparison between GDP energies and HYCOM ones, both data processing methods were compared with LLC4320 data. Observed differences are mostly noise-like and lower than differences reported in section 2 (2% due to the noise in average against 6% caused by the difference of dataset).

High Resolution Empirical Tide (HRET)

HRET processing is described in Zaron (2019) and Zaron et al. (2022). HRET is an internal tide atlas based on satellite altimetric data mapping the sea surface height (SSH) associated with internal tides component (Zaron, 2019; Zaron et al., 2022). Estimation of variance are obtained for the M_2 coherent IT signal. To this signal we added an estimation of the variance of the S_2 coherent IT using theoretical equilibrium tides amplitudes.

$$KE = KE_{M_2}(1 + \frac{a_{S_2}}{a_{M_2}}) \tag{3}$$

where KE_{M_2} is the energy estimation from HRET, a_{S_2} is the equilibrium amplitude of S_2 and a_{M_2} is the equilibrium amplitude of M_2.

The estimation of energy based on HRET accounts for the coherent signal of two tidal components, M_2 and S_2. HRET thus provides a fraction of the signal that can be obtained via integrated spectra or bandpass filtering, and is therefore expected to provide lower energy levels compared to data sources that account for the full tidal signal (e.g. LLC4320, HYCOM, GDP). The comparison between HRET diagnostics and other data sources highlights the fraction of internal tide energy not represented in satellite climatologies.

Predicting apparent incoherence

In section 2, we present a prediction of the Lagrangian to Eulerian energy ratio. This prediction is based on the study developed in Caspar-Cohen et al. (2022) which provides a theoretical model for the Lagrangian autocorrelation, following:

$$\tilde{C}_L(\tau) = \tilde{C}_E(\tau)e^{-k^2\sigma^2(\tau)} \tag{4}$$

where $\tilde{C}(\tau)$ is the Eulerian autocovariance, k the internal tide horizontal wavenumber and σ a prediction of drifters' displacement depending on the low frequency motion amplitude and decorrelation timescale. Internal tides and low frequency motion properties (energy and decorrelation timescales) are estimated from the Eulerian outputs of LLC4320 simulation, following the fitting method described in Caspar-Cohen et al. (2022). From these Eulerian estimates, Eulerian autocovariance is computed, and the Lagrangian autocovariance predicted.

Eulerian and Lagrangian spectra, noted $\tilde{E}_e$ and $\tilde{E}_l$ respectively, are then estimated via their relationship with autocovariance functions:

$$E(\omega) = \int_{-\infty}^{\infty} C(\tau) cos(\omega\tau) d\tau \tag{5}$$

where C is an autocovariance function. Estimates of the Eulerian and Lagrangian energy fields can then be inferred from these spectra by integration in a fixed bandwidth.

$$KE_{E,high} = \int_{\omega_c-\Delta\omega/2}^{\omega_c+\Delta\omega/2} \tilde{E}_e(\omega) d\omega, \tag{6}$$

$$KE_{L,high,predicted} = \int_{\omega_c-\Delta\omega/2}^{\omega_c+\Delta\omega/2} \tilde{E}_l(\omega) d\omega \tag{7}$$

where ω_c is the central frequency of the filter and $\Delta\omega$ its bandwidth. Consequently the energy ratio referred to as "predicted energy ratio" in section 2 corresponds to $KE_{L,high,predicted}/KE_{E,high}$ (Figure 2a and 2b) and is compared to the "estimated energy ratio", $KE_{L,high}/KE_{E,high}$ (Figure 2c and 2d).

References

Ansong, J. K., Arbic, B. K., Buijsman, M. C., Richman, J. G., Shriver, J. F., and Wallcraft, A. J. (2015). Indirect evidence for substantial damping of low-mode internal tides in the open ocean. *Journal of Geophysical Research: Oceans*, 120(9):6057–6071.

Arbic, B. K. (2022). Incorporating tides and internal gravity waves within global ocean general circulation models: A review. *Progress in Oceanography*, page 102824.

Arbic, B. K., Alford, M. H., Ansong, J. K., Buijsman, M. C., Ciotti, R. B., Farrar, J. T., Hallberg, R. W., Henze, C. E., Hill, C. N., Luecke, C. A., et al. (2018). Primer on global internal tide and internal gravity wave continuum modeling in hycom and mitgcm. *New frontiers in operational oceanography*, pages 307–392.

Arbic, B. K., Elipot, S., Brasch, J. M., Menemenlis, D., Ponte, A. L., Shriver, J. F., Yu, X., Zaron, E. D., Alford, M. H., Buijsman, M. C., et al. (2022). Near-surface oceanic kinetic energy distributions from drifter observations and numerical models. *Journal of Geophysical Research: Oceans*, 127(10):e2022JC018551.

Arbic, B. K., Lyard, F., Ponte, A., Ray, R. D., Richman, J. G., Shriver, J. F., Zaron, E., and Zhao, Z. (2015). Tides and the SWOT mission: Transition from Science Definition Team to Science Team. *Civ. Environ. Eng. Fac. Publ. Present.*, page 10.

Arbic, B. K., Wallcraft, A. J., and Metzger, E. J. (2010). Concurrent simulation of the eddying general circulation and tides in a global ocean model. *Ocean Modelling*, 32(3-4):175–187.

Buijsman, M. C., Stephenson, G. R., Ansong, J. K., Arbic, B. K., Green, J. M., Richman, J. G., Shriver, J. F., Vic, C., Wallcraft, A. J., and Zhao, Z. (2020). On the interplay between horizontal resolution and wave drag and their effect on tidal baroclinic mode waves in realistic global ocean simulations. *Ocean Modelling*, 152:101656.

Caspar-Cohen, Z., Ponte, A., Lahaye, N., Carton, X., Yu, X., and Gentil, S. L. (2022). Characterization of internal tide incoherence: Eulerian versus lagrangian perspectives. *Journal of Physical Oceanography*, 52(6):1245–1259.

de Lavergne, C., Falahat, S., Madec, G., Roquet, F., Nycander, J., and Vic, C. (2019). Toward global maps of internal tide energy sinks. *Ocean Modelling*, 137:52–75.

Delandmeter, P. and Van Sebille, E. (2019). The parcels v2. 0 lagrangian framework: new field interpolation schemes. *Geoscientific Model Development*, 12(8):3571–3584.

Elipot, S., Lumpkin, R., Perez, R. C., Lilly, J. M., Early, J. J., and Sykulski, A. M. (2016). A global surface drifter data set at hourly resolution. *Journal of Geophysical Research: Oceans*, 121(5):2937–2966.

Elipot, S., Sykulski, A., Lumpkin, R., Centurioni, L., and Pazos, M. (2022). Hourly location, current velocity, and temperature collected from global drifter program drifters world-wide. *NOAA National Centers for Environmental Information.*

Ferrari, R. and Wunsch, C. (2009). Ocean circulation kinetic energy: Reservoirs, sources, and sinks. *Annual Review of Fluid Mechanics*, 41:253–282.

Geoffroy, G. and Nycander, J. (2022). Global Mapping of the Nonstationary Semidiurnal Internal Tide Using Argo Data. *JGR Oceans*, 127(4).

LaCasce, J. (2008). Statistics from lagrangian observations. *Progress in Oceanography*, 77(1):1–29.

Lahaye, N., Gula, J., and Roullet, G. (2019). Sea surface signature of internal tides. *Geophysical Research Letters*, 46(7):3880–3890.

Le Guillou, F., Lahaye, N., Ubelmann, C., Metref, S., Cosme, E., Ponte, A., Le Sommer, J., Blayo, E., and Vidard, A. (2021a). Joint estimation of balanced motions and internal tides from future wide-swath altimetry. *Journal of Advances in Modeling Earth Systems*, 13(12):e2021MS002613.

Le Guillou, F., Metref, S., Cosme, E., Ubelmann, C., Ballarotta, M., Le Sommer, J., and Verron, J. (2021b). Mapping altimetry in the forthcoming swot era by back-and-forth nudging a one-layer quasigeostrophic model. *Journal of Atmospheric and Oceanic Technology*, 38(4):697–710.

Luecke, C. A., Arbic, B. K., Richman, J. G., Shriver, J. F., Alford, M. H., Ansong, J. K., Bassette, S. L., Buijsman, M. C., Menemenlis, D., Scott, R. B., et al. (2020). Statistical comparisons of temperature variance and kinetic energy in global ocean models and observations: Results from mesoscale to internal wave frequencies. *Journal of Geophysical Research: Oceans*, 125(5):e2019JC015306.

Melet, A., Hallberg, R., Legg, S., and Polzin, K. (2013). Sensitivity of the ocean state to the vertical distribution of internal-tide-driven mixing. *Journal of Physical Oceanography*, 43(3):602–615.

Melet, A., Legg, S., and Hallberg, R. (2016). Climatic impacts of parameterized local and remote tidal mixing. *Journal of Climate*, 29(10):3473–3500.

Munk, W. and Wunsch, C. (1998). Abyssal recipes ii: Energetics of tidal and wind mixing. *Deep Sea Research Part I: Oceanographic Research Papers*, 45(12):1977–2010.

NASA, J. (2021). Pre-swot level-4 hourly mitgcm llc4320 native 2km grid oceanographic version 1.0.

Nelson, A. D., Arbic, B. K., Zaron, E. D., Savage, A. C., Richman, J. G., Buijsman, M. C., and Shriver, J. F. (2019). Toward realistic nonstationarity of semidiurnal baroclinic tides in a hydrodynamic model. *Journal of Geophysical Research: Oceans*, 124(9):6632–6642.

Olbers, D., Eden, C., Becker, E., Pollmann, F., and Jungclaus, J. (2019). The idemix model: Parameterization of internal gravity waves for circulation models of ocean and atmosphere. *Energy Transfers in Atmosphere and Ocean*, pages 87–125.

Pan, H., Jiao, S., Xu, T., Lv, X., and Wei, Z. (2022). Investigation of tidal evolution in the bohai sea using the combination of satellite altimeter records and numerical models. *Estuarine, Coastal and Shelf Science*, 279:108140.

Ray, R. D. and Mitchum, G. T. (1996). Surface manifestation of internal tides generated near hawaii. *Geophysical Research Letters*, 23(16):2101–2104.

Ray, R. D. and Mitchum, G. T. (1997). Surface manifestation of internal tides in the deep ocean: Observations from altimetry and island gauges. *Progress in Oceanography*, 40(1-4):135–162.

Rocha, C. B., Chereskin, T. K., Gille, S. T., and Menemenlis, D. (2016). Mesoscale to submesoscale wavenumber spectra in drake passage. *Journal of Physical Oceanography*, 46(2):601–620.

Simmons, H. L., Jayne, S. R., Laurent, L. C. S., and Weaver, A. J. (2004). Tidally driven mixing in a numerical model of the ocean general circulation. *Ocean Modelling*, 6(3-4):245–263.

Timko, P. G., Arbic, B. K., Richman, J. G., Scott, R. B., Metzger, E. J., and Wallcraft, A. J. (2012). Skill tests of three-dimensional tidal currents in a global ocean model: A look at the north atlantic. *Journal of Geophysical Research: Oceans*, 117(C8).

Timko, P. G., Arbic, B. K., Richman, J. G., Scott, R. B., Metzger, E. J., and Wallcraft, A. J. (2013). Skill testing a three-dimensional global tide model to historical current meter records. *Journal of Geophysical Research: Oceans*, 118(12):6914–6933.

Van Sebille, E., Griffies, S. M., Abernathey, R., Adams, T. P., Berloff, P., Biastoch, A., Blanke, B., Chassignet, E. P., Cheng, Y., Cotter, C. J., et al. (2018). Lagrangian ocean analysis: Fundamentals and practices. *Ocean Modelling*, 121:49–75.

Wang, H., Grisouard, N., Salehipour, H., Nuz, A., Poon, M., and Ponte, A. L. (2022). A deep learning approach to extract internal tides scattered by geostrophic turbulence. *Geophysical Research Letters*, 49(11):e2022GL099400.

Wang, J., Fu, L.-L., Qiu, B., Menemenlis, D., Farrar, J. T., Chao, Y., Thompson, A. F., and Flexas, M. M. (2018). An observing system simulation experiment for the calibration and validation of the surface water ocean topography sea surface height measurement using in situ platforms. *Journal of Atmospheric and Oceanic Technology*, 35(2):281–297.

Whalen, C. B., de Lavergne, C., Garabato, A. C. N., Klymak, J. M., Mackinnon, J. A., and Sheen, K. L. (2020). Internal wave-driven mixing: governing processes and consequences for climate. *Nature Reviews Earth & Environment*, 1(11):606–621.

Yu, X., Ponte, A. L., Elipot, S., Menemenlis, D., Zaron, E. D., and Abernathey, R. (2019). Surface Kinetic Energy Distributions in the Global Oceans From a High-Resolution Numerical Model and Surface Drifter Observations. *Geophys. Res. Lett.*, 46(16):9757–9766.

Zaron, E. D. (2017). Mapping the nonstationary internal tide with satellite altimetry. *J. Geophys. Res. Oceans*, 122(1):539–554.

Zaron, E. D. (2019). Baroclinic tidal sea level from exact-repeat mission altimetry. *Journal of Physical Oceanography*, 49(1):193–210.

Zaron, E. D. and Elipot, S. (2021). An assessment of global ocean barotropic tide models using geodetic mission altimetry and surface drifters. *Journal of Physical Oceanography*, 51(1):63–82.

Zaron, E. D., Musgrave, R. C., and Egbert, G. D. (2022). Baroclinic tidal energetics inferred from satellite altimetry. *Journal of Physical Oceanography*, 52(5):1015–1032.

Zhao, Z. (2014). Internal tide radiation from the luzon strait. *Journal of Geophysical Research: Oceans*, 119(8):5434–5448.

Zhao, Z., Alford, M. H., and Girton, J. B. (2012). Mapping low-mode internal tides from multisatellite altimetry. *Oceanography*, 25(2):42–51.

Authors contributions

Z.C-C., A.P. and N.L. designed the data processing of LLC4320 and GDP data as well as analysis presented in the manuscript. Manuscript was primarily written by Z.C.C. and numerical simulation of drifters designed by A.P. E.D.Z. provided the energy estimates from HRET. B.K.A provided the estimates from HYCOM. X.Y. contributed to initial LLC4320 data processing and analysis. Sylvie LeGentil contributed to the numerical simulation of drifters. Dimitris Menemenlis provided the LLC4320 outputs. All authors participated to the scientific discussion and reviewing of the manuscript.

Acknowledgment

N.L. and Z.C-C. received fundings from the French National Research Agency (ANR) through the Mod-ITO project "ANR-22-CE01-0006-01", and A.P., Z.L and Z.C-C. acknowledge support from the TOSCA-ROSES SWOT project DIEGO. E.D.Z. acknowledges support from NSF Grant OCE-1850961 and NASA Grant 80NSSC21K0346. B.K.A. acknowledges support from US National Science Foundation (NSF) Grant OCE-1851164, US Office of Naval Research (ONR) Grant N00014-18-1-2544, and NASA Grant 80NSSC20K1135. X.Y. acknowledges support from the National Natural Science Foundation of China (Grants 42206002, 42361144844), and Guangdong Basic and Applied Basic Research Foundation (2023A1515010654).

Data availability

The IT energy levels estimated from LLC4320 and GDP datasets are provided at, `https://doi.org/10.5281/zenodo.10851200`. The HRET tide model is available to reviewers at the URL, `https://ingria.ceoas.oregonstate.edu/fossil/SMCE/dir?ci=tip`. A manuscript describing the model is under review at JTech. A DOI for the model will be provided if this manuscript is accepted. The Matlab code used to process HYCOM outputs and the results used in this paper are provided in Arbic et al. (2022); `https://doi.org/10.7302/PTG7-YW20`.

List of Figures

Supplementary Files

This is a list of supplementary files associated with this preprint. Click to download.

- Suppinformation.pdf